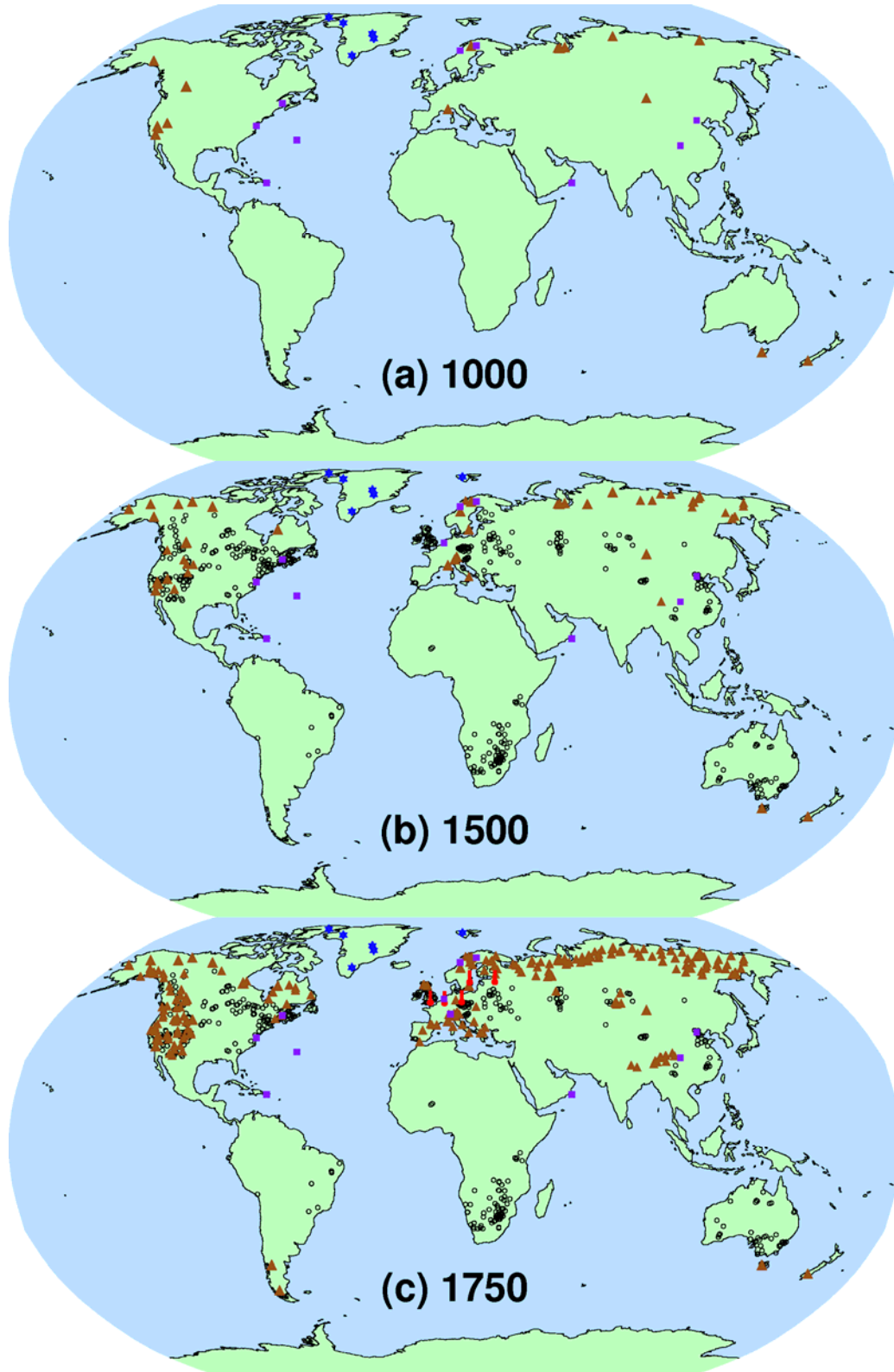


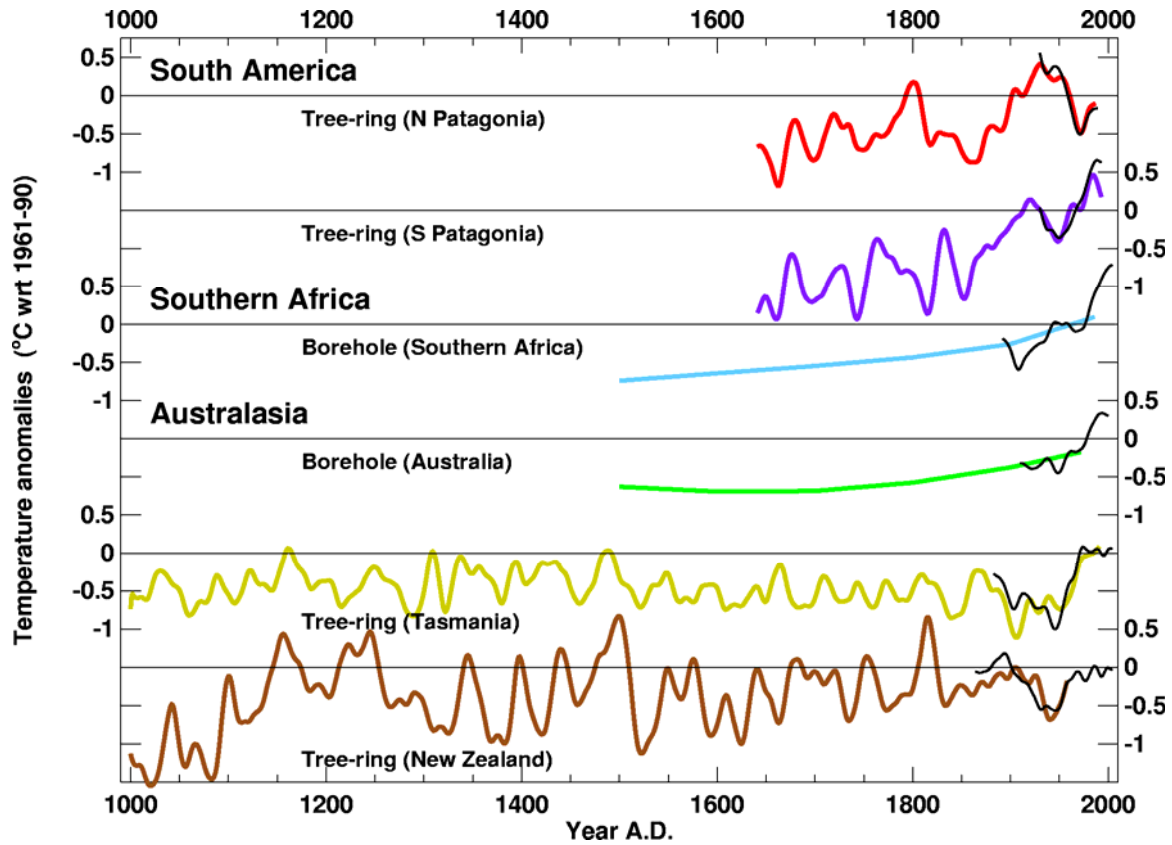
1
2



3
4
5
6
7
8
9
10

Figure 6.11. Locations of temperature-sensitive proxy records with data back to 1000, 1500 and 1750 (instrumental records: red thermometers; tree-ring: brown triangles; boreholes: black circles; ice-core/ice-boreholes: blue stars; other records including low-resolution records: purple squares). All proxies used in reconstructions [R1] to [R11] of Northern Hemisphere temperatures (see Table 6.1 and Figure 6.10) or used to indicate Southern Hemisphere regional temperatures (Figure 6.12) are included.

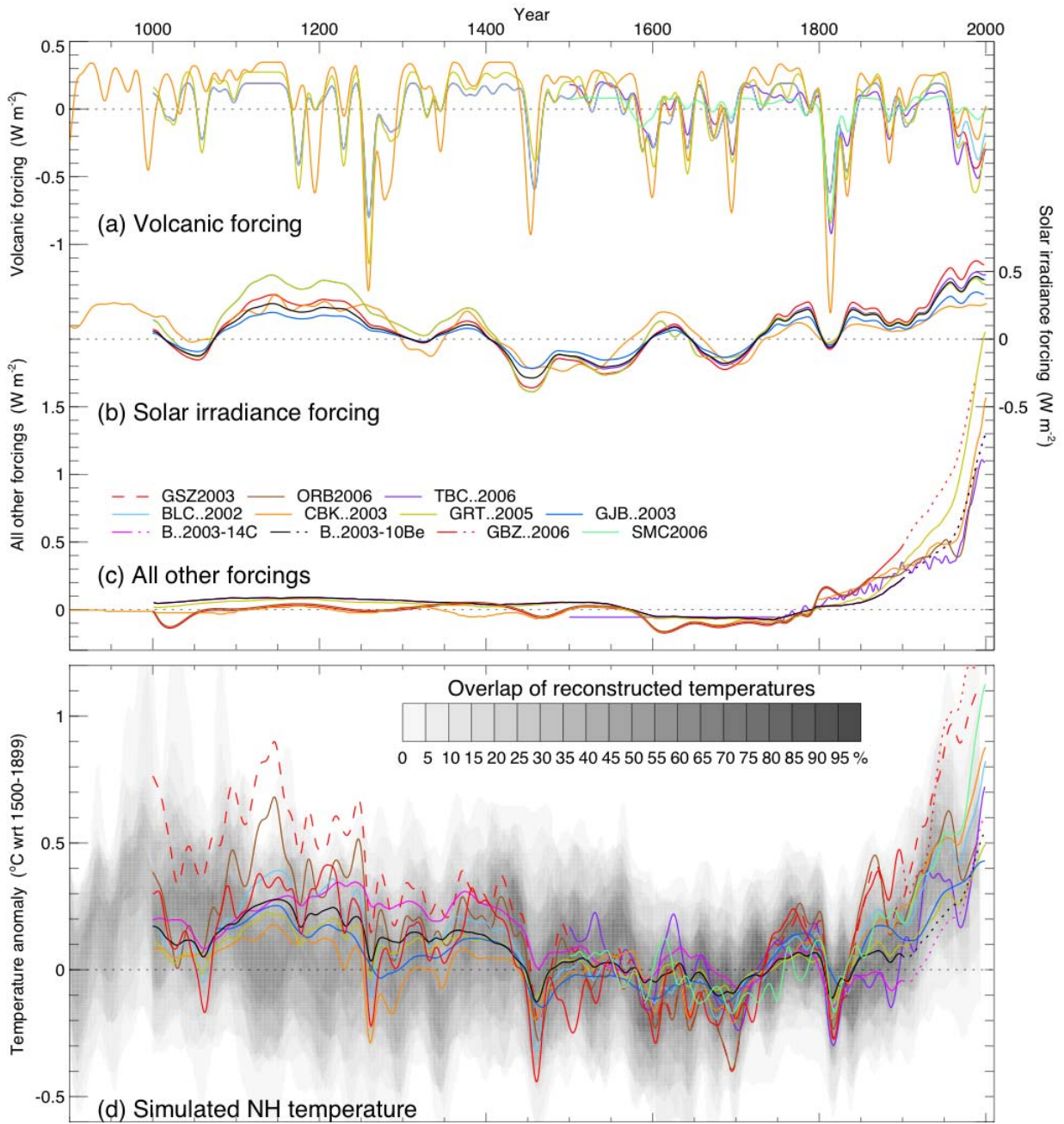
1
2



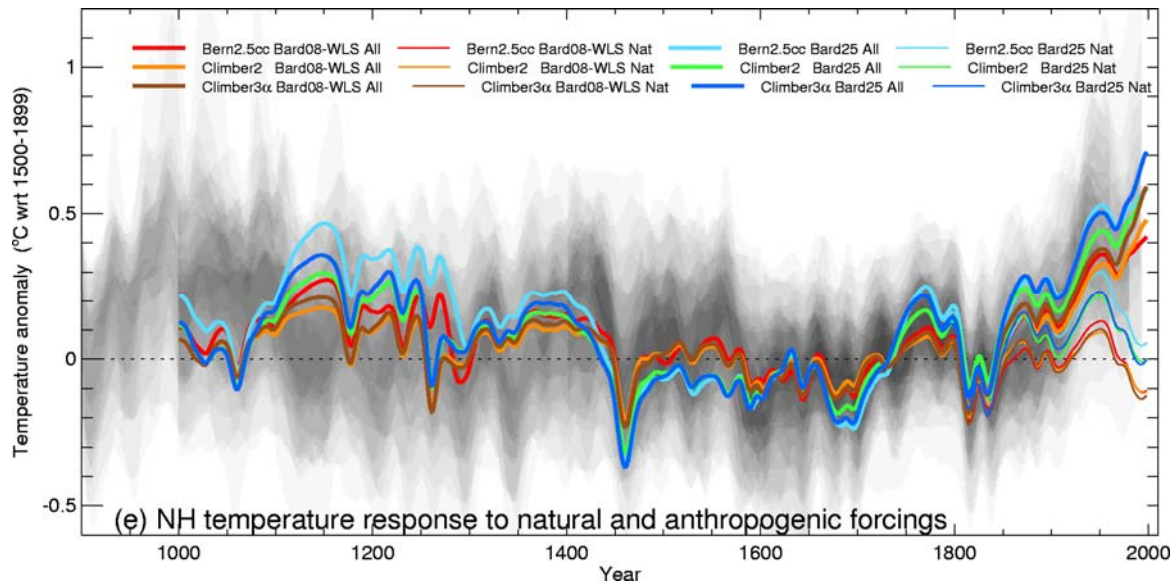
3
4
5
6
7
8
9
10
11
12

Figure 6.12. Temperature reconstructions for regions in the Southern Hemisphere: two annual temperature series from South American tree-ring data (Villalba et al., 2003); annual temperature estimates from borehole inversions for southern Africa and Australia (derived using the approach of Pollock and Smerdon (2004); summer temperature series from Tasmania and New Zealand tree-ring data (Cook et al., 2000; Cook et al., 2002a). The black curves show summer or annual instrumental temperatures for each region. All tree-ring and instrumental series have been smoothed with a 25-year filter and represent anomalies ($^{\circ}\text{C}$) from the 1961–1990 mean (indicated by the horizontal lines).

1



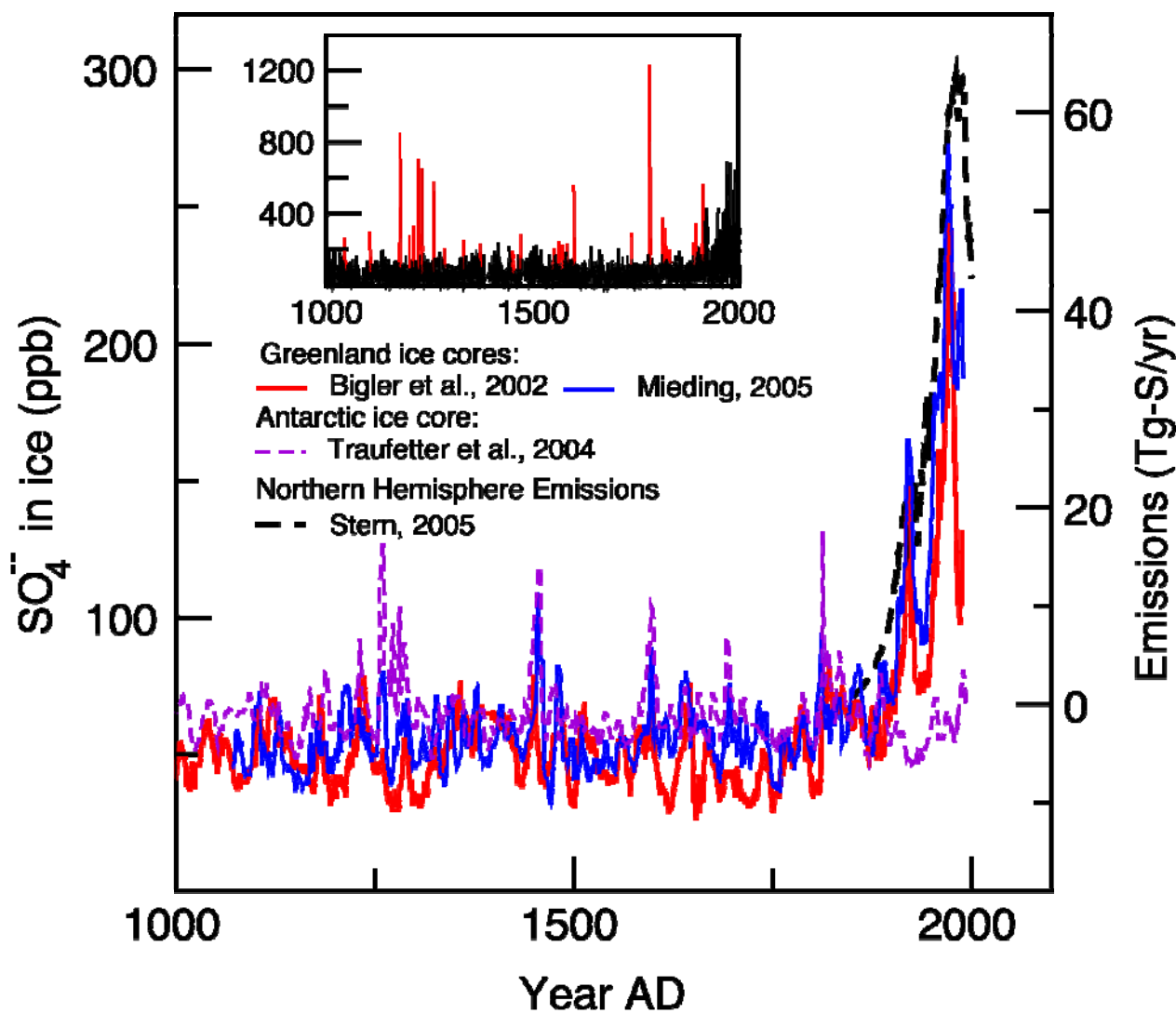
2



1
 2 **Figure 6.13.** Radiative forcings and simulated temperatures during the last 1100 years. Global-mean
 3 radiative forcing (W m^{-2}) used to drive climate model simulations due to (a) volcanic activity, (b) solar
 4 irradiance variations (these values are indicated by the labeling on the right-hand axis), and (c) all other
 5 forcings (which vary between models, but always include greenhouse gases and, except for those with dotted
 6 lines after 1900, tropospheric sulphate aerosols). Annual-mean NH temperature ($^{\circ}\text{C}$) simulated (d) under the
 7 range of forcings shown in (a)-(c) and (e) in a set of experiments designed to isolate the influences of
 8 anthropogenic and natural forcings, for two different estimates of solar irradiance variability ('All' [thick]
 9 used anthropogenic and natural forcings, 'Nat' [thin] used only natural forcings). The region of overlapping
 10 NH temperature reconstructions is shown by grey shading in panels (d) and (e) (modified from Figure 6.11c
 11 to account for the 1500–1899 reference period used here).

12
 13 All forcings and temperatures are expressed as anomalies from their 1500–1899 means and then smoothed
 14 with a Gaussian-weighted filter to remove fluctuations on time scales less than 30 years; smoothed values are
 15 obtained up to both ends of each record by extending the records with the mean of the adjacent existing
 16 values.

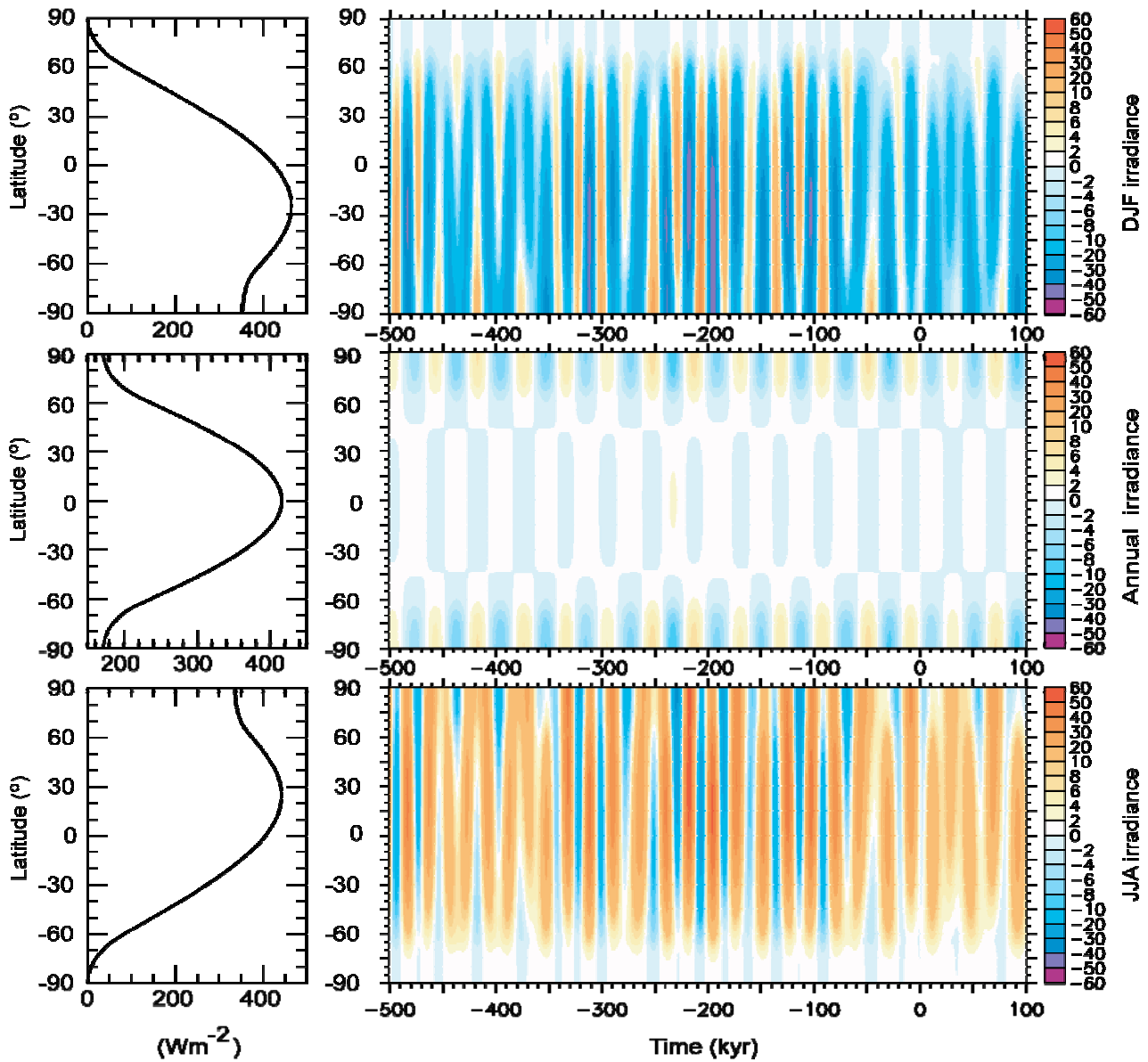
17
 18 The individual series are defined in Table 6.2 for (a) to (d), and in Table 6.3 for (e).
 19



1
2
3
4
5
6
7
8
9

Figure 6.14. Sulfate concentrations in Greenland and Antarctic ice cores (Fischer et al., 1998; Bigler et al., 2002; Mieding, 2005) during the last millennium. Also shown are the estimated anthropogenic sulfur emissions for the Northern Hemisphere (Stern, 2005). The ice core data have been smoothed with a 10-year running median filter, thereby removing the peaks of major volcanic eruptions. The inset illustrates the influence of volcanic emissions and shows monthly data as measured (red) and with the volcanic spikes removed (black) (Bigler et al., 2002).

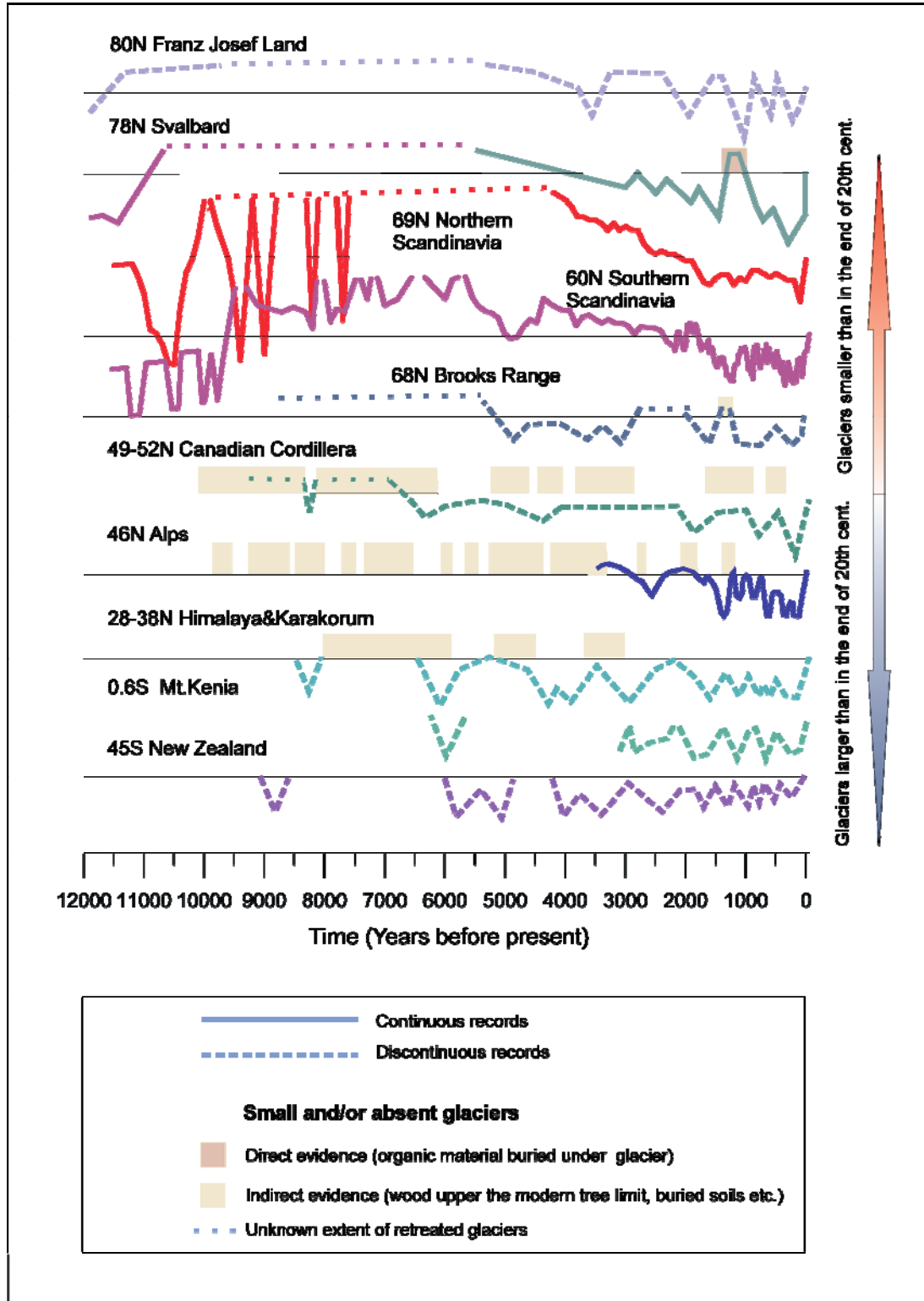
1
2



3
4
5
6
7
8
9
10
11

Box 6.1, Figure 1. December-January-February (top panel), annual mean (middle panel) and June-July-August (bottom panel) latitudinal distribution of present-day (year 1950) incoming mean solar radiation ($W m^{-2}$). Right side: deviations with respect to present-day of December-January-February (top panel), annual mean (middle panel) and June-July-August (bottom panel) latitudinal distribution of incoming mean solar radiation from the past 500 kyr to the future 100 kyr (W/m^{-2}) (Berger and Loutre, 1991; Loutre et al., 2004).

1
2



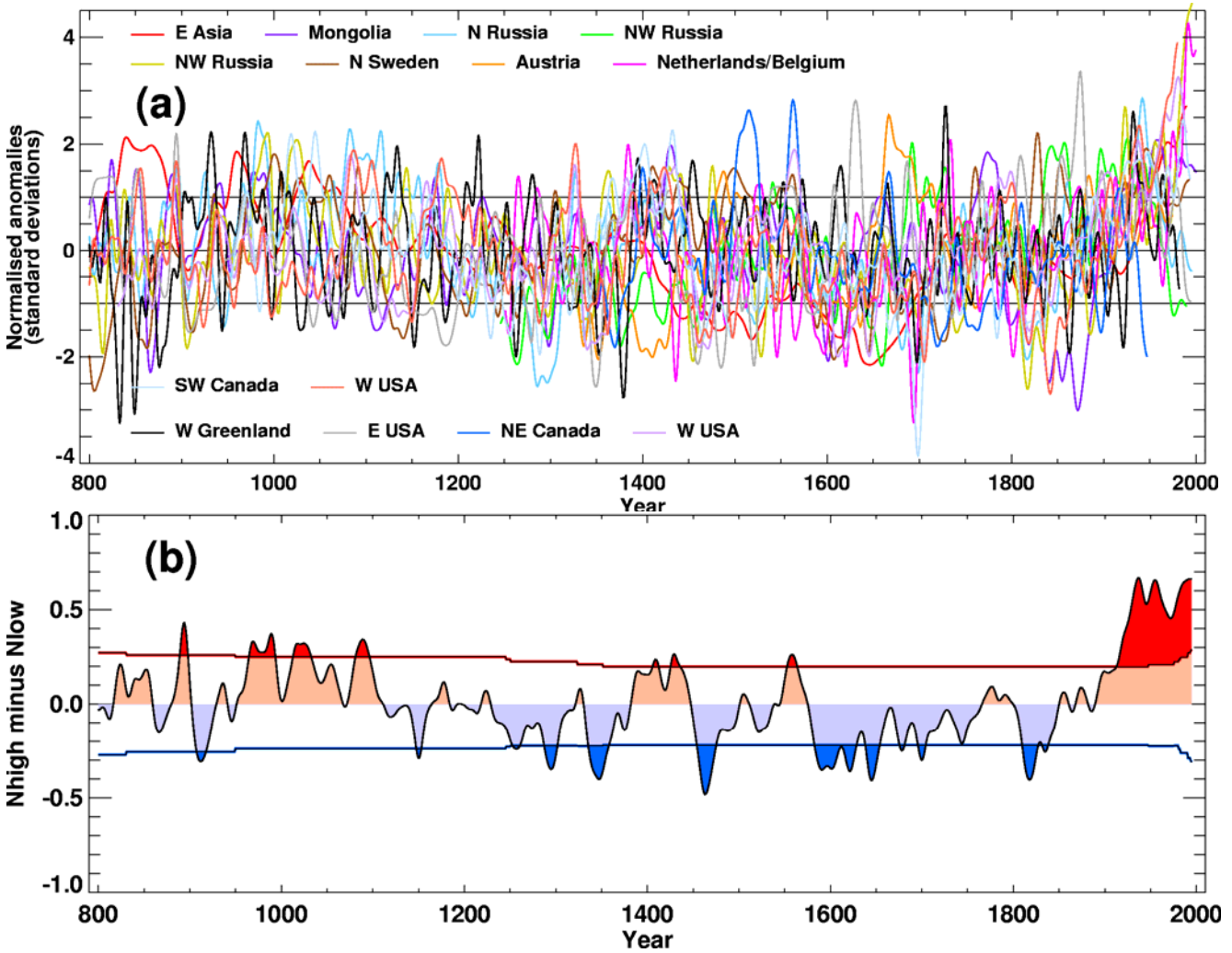
3
4
5
6
7
8
9
10
11
12

Box 6.3, Figure 1.

Franz Josef Land – (Lubinski et al., 1999), calibrated.
 Svalbard – curve from (Svendsen and Mangerud, 1997) corrected with (Humlum et al., 2005).
 Northern Scandinavia (Nesje et al, 2005; Bakke et al., 2005a; Bakke et al., 2005c).
 Southern Scandinavia (Dahl et al, 1996; Matthews et al., 2000; Lie et al., 2004; Matthews et al., 2005).
 Brooks Range – (Ellis and Calkin, 1984), calibrated.
 Canadian Cordillera – (Luckman and Kearney, 1986; Osborn and Luckman, 1988), calibrated, (Koch et al., 2004; Menounos et al., 2004).

- 1 Alps – (Holzhauser et al., 2005; Joerin et al., accepted 2005).
- 2 Himalaya and Karakorum – (Roethlisberger and Geyh, 1985), calibrated, (Bao et al., 2003).
- 3 Mt Kenya – (Karlen et al., 1999).
- 4 New Zealand – (Gellatly et al., 1988), calibrated.

1
2



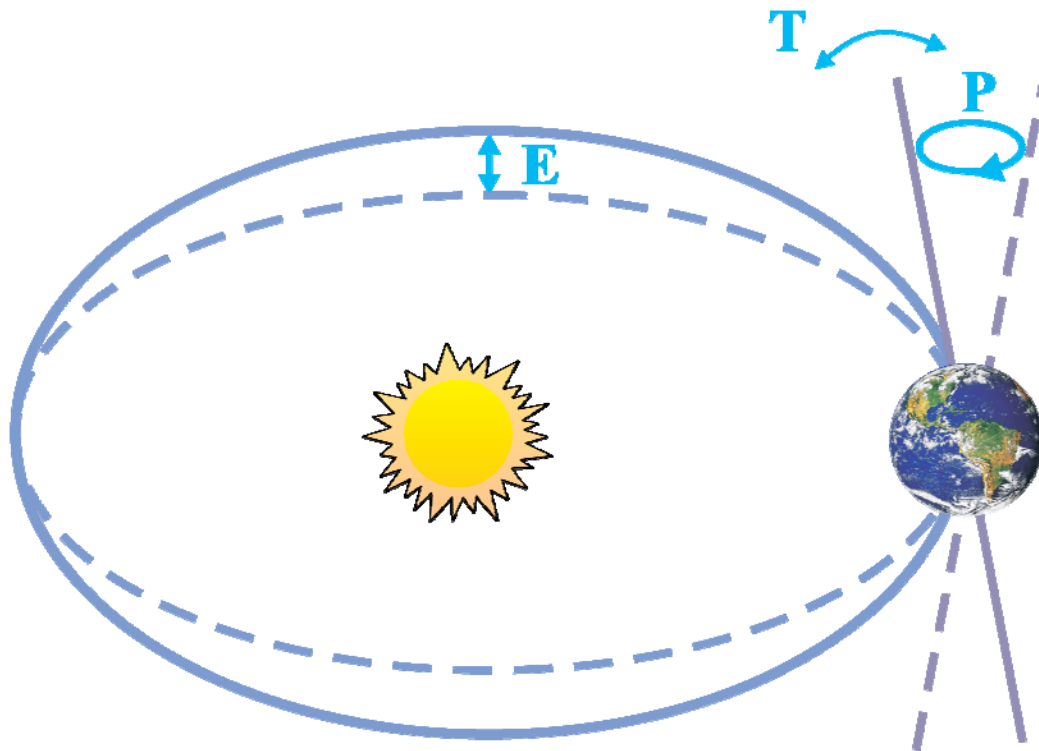
3

4
5

Box 6.4, Figure 1. (a) The heterogeneous nature of climate during the MWP is illustrated by the wide spread of values exhibited by the individual records that have been used to reconstruct NH-mean temperature. Individual, or small regional averages of, proxy records used in various studies (see Osborn and Briffa, 2006), (collated from those used by Mann and Jones (2003), Esper et al. (2002) and Luckman and Wilson (2005) but excluding shorter series or those with an ambiguous relationship to local temperature). These records have not been calibrated (though all show positive correlations with local temperature observations), but have been smoothed with a 20-year filter and scaled to have zero mean and unit standard deviation over the period 800–1995.

(b) The fraction of records shown in (a) that exceed the +1 standard deviation line, minus the fraction of records that are below the -1 standard deviation line (Osborn and Briffa, 2006). Horizontal lines indicate periods when the results differ significantly from those expected if the time series had no relationship to temperature (specifically, the 5th and 95th percentiles of the distributions of results obtained after shifting individual records randomly in time, thus destroying the calendar alignment between records).

20

1
23
4
5
6
7
8
9

Question 6.1, Figure 1. Schematic of the Earth's orbital changes (Milankovitch cycles) that drive the ice age cycles. "T" denotes changes in the tilt (or obliquity) of the Earth axis, "E" denotes changes in the eccentricity of the orbit, and "P" denotes precession, i.e., changes in the direction of the axis tilt at a given point of the orbit. Source: Rahmstorf and Schellnhuber (2006).